

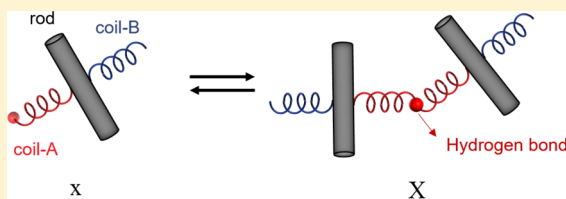
Archimedean Tiling Patterns Self-Assembled from X-Shaped Rod–Coil Copolymers with Hydrogen Bonds

Faqiang Liu, Ping Tang,*^{ID} Hongdong Zhang, and Yuliang Yang

State Key Laboratory of Molecular Engineering of Polymers, Department of Macromolecular Science, Fudan University, Shanghai 200433, China

Supporting Information

ABSTRACT: On the basis of self-consistent field theory (SCFT), we demonstrate that X-shaped rod–coil molecules with hydrogen-bonding groups self-assemble into Archimedean tiling patterns including [3⁶], [4⁴], [6³], [3.4.6.4], and [(3.6)²], and dual tiling patterns including dual-[3².4.3.4]. The rod blocks form the edges of polygons, coil blocks fill in the inner spaces of polygons, and the existence of hydrogen bonds further decreases the domain size. A new mechanism is proposed to guide the formation of Archimedean tiling patterns: the fabrication of tiling patterns is controlled by the relationship between the length–diameter ratio β and volume fraction f_R of rigid cores in X-shaped supra-macromolecules. This study provides a concept of macromolecular tiling for producing Archimedean tilings and suggests X-shaped rod–coil supra-macromolecules with hydrogen-bonding groups as an ideal platform for the fabrication of two-dimensional nanoscale patterns.



INTRODUCTION

Archimedean tilings made by convex regular polygons have been widely used since antiquity. They were first systematically and mathematically treated by Kepler.¹ Although first proposed as a geometrical problem, these tilings composed of various polygons are also widely used in crystallography, polymer science, etc. Most crystal structures and some quasicrystals^{2,3} can be decomposed into different tilings, such as the local [3².4.3.4] tiling (a tiling is named by the order of polygons surrounding one vertex in a circle order; 3² means two triangles (see Figure S1 for details)) in Frank–Kasper phase.² Archimedean tiling patterns self-assembled by polymers are not only directly applied in microelectronic and optoelectronic devices,⁴ displays, biochips, photonic band gap materials,⁵ and sensors,⁶ but also indirectly used as substrates^{7,8} or pattern masks⁹ in superconducting technology.

Archimedean tilings with identical vertexes (Figure S1) can be obtained by lithography,⁸ direct synthesis of organic and inorganic materials,^{10,11} and self-assembly of DNA¹² and block copolymers (BCPs).¹³ BCPs are promising materials for fabricating low-cost and diverse large-scale controllable tiling patterns. We reported [4⁴] and [4.8²] tilings formed by ABC linear and star triblock copolymers theoretically using self-consistent field theory (SCFT);^{14,15} they were later obtained experimentally by Haruko et al.¹³ The scale of microphase separation domains in tiling patterns assembled from traditional BCPs is generally more than 30 nm. However, the performance of these devices generally decreases with increasing domain size; thus, the oversized microstructures of BCPs limit applications in many fields such as the semiconductor industry. Copolymers with strong chemical repulsions¹⁶ and different macromolecular topologies¹⁷ were

used to tune the smaller domain size; however, these methods reduced the flexibility of BCPs, thus canceling out the advantages of BCPs. Other than the tiling patterns formed by BCPs where the interfaces of different domains serve as the edges of polygons, the patterns can also be formed by a special type of BCPs: T/X-shaped molecules with hydrogen-bonding groups (Figure 1), where the rod blocks construct the edges of

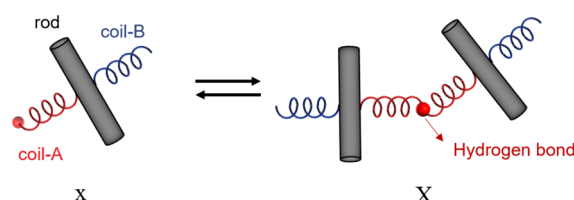


Figure 1. Schematic representation of X-shaped rod–coil molecules x forming supra-macromolecule X via hydrogen-bonding groups at the terminal segment of coil-A blocks. The reactant molecule x contains one rigid core (rod) and two flexible side chains (coil-A and coil-B) attached at the middle of the rod. The X-shaped molecule turns into T-shaped molecule if coil-B is removed.

polygons and side chains fill the inner spaces.^{18–21} The additional introduction of hydrogen bonds can further narrow down the domain sizes to as small as 5 nm,²¹ thus making X/T-shaped rod–coil molecules satisfying the three most needed characteristics of tilings in polymer industry: low cost, easy morphology control, and performance guarantee.

Received: May 24, 2018

Revised: September 12, 2018

Published: September 26, 2018

Unfortunately, both traditional BCPs and T/X-shaped molecules only self-assemble to form limited tiling patterns. Until now, only [4.8²], [4⁴], [4.6.12], [3².4.3.4], dual-[3².4.3.4], and [6³] tilings were obtained from traditional BCPs, and [3⁶], [4⁴], [6³], [3².4.3.4], and [(3.6)²] tilings were obtained using T/X-shaped molecules. Moreover, many theoretical^{22–25} and experimental investigations^{26,27} predicted the formation of diverse tilings and found out some empirical rules to guide the formation. However, these works mainly consider the length of rigid cores with constant diameter or the volume of lateral chains (equivalent to the volume fraction of rods in the present work) due to synthetic challenges or heavy computational loads; these qualitative mechanisms are not enough to guide the fabrication of targeted tiling patterns. Therefore, a general quantitative or semiquantitative analysis is essential to guide the macromolecular design for self-assembly of Archimedean tiling patterns. Because of the high dimensionality of parameter space, the demands cannot be satisfied by exploring the self-assembly behavior after synthesizing a macromolecule in experiments. Therefore, a combination of theory and experiments to derive a general principle to obtain the target tiling pattern is a rational choice. In this study, X-shaped rod-coil macromolecules with hydrogen-bonding groups are used to explore the feasibility of preparing 11 kinds of Archimedean tilings (Figure S1) using SCFT calculations.

THEORY AND METHOD

Considering an incompressible melt of X-shaped original molecules x (left panel of Figure 1) with volume V, the coil-A and coil-B blocks are modeled as Gaussian chains with lengths N_A and N_B, respectively, and the rigid cores are modeled as rigid rods with length N_R. The hydrogen-bonding groups at the terminal segments of coil-A can reversibly connect to each other, forming supra-macromolecules X (right panel in Figure 1). The reversible reaction can be expressed as follows:



When the equilibrium is reached

$$\mu_x = 2\mu_x \quad (2)$$

where μ_m is the chemical potential of molecule m ($m \in \{x, X\}$). We formulate our model in the grand canonical ensemble for fixed activity, volume, and temperature. As the field-theoretic method of rod-coil BCPs has been described in our previous study,²⁸ the complete SCFT derivations are not shown here. In present work, the supramolecular diblock copolymer (SDC) model describing hydrogen bonds proposed by Feng et al.²⁹ is used to describe the hydrogen-bond interactions. Therefore, only the theoretical treatment of the reaction in eq 1 is demonstrated. In the thermodynamics of chemical reactions, the chemical potentials of molecules x and X are

$$\mu_x = G_x^0 + \ln z_x \quad (3)$$

$$\mu_X = G_X^0 - F_B + \ln z_X \quad (4)$$

where F_B is the free energy change when a hydrogen bond is formed and G_m^0 is the Gibbs free energy of single m molecular chain in the standard state which satisfies

$$G_m^0 = -\ln(Q_m^0/\lambda_T^{3N_m}) \quad (5)$$

Q_m^0 is the unnormalized single m chain partition functions in zero fields, and λ_T is the thermal wavelength.³⁰ Similar to the derivation of Feng et al.,²⁹ we obtain

$$Q_x^0 = V_x g_R^{N_R} g_M^{N_A+N_B-1} \quad (6)$$

$$Q_X^0 = V_x g_R^{2N_R} g_M^{2N_A+2N_B-1} \quad (7)$$

where g_M and g_R are the monomer volumes of coil and rod, respectively, independent of the chain length.³⁰ V_m is the volume occupied by one m chain and can be written as $V_m = N_m v_0$,³¹ and v_0 is the volume of one segment. From eqs 2–7, we obtain

$$z_x = z_x^2 e^{-F_B} \frac{4\rho_0 g_M}{N} \quad (8)$$

where z_m is the dimensionless activity of m molecule in unit of ρ_0/N , $\rho_0 = \sum_m n_m N_m / V = 1/v_0$, and n_m and N_m are the number and the chain length of m molecules, respectively. $N = N_x = 2N_x = 2\sum_i N_i$ ($i \in \{A, B, R\}$). Under the incompressible condition, we set $z_x = 1$. By absorbing $4\rho_0 g_M$ into F_B , we get

$$z_x = e^{-F_B} N^{-1} \quad (9)$$

where $F_B = F_B - \ln 4\rho_0 g_M$. The grand canonical Hamiltonian H_g scaled by the reference number of polymer chains $\rho_0 V / N$ can be expressed by

$$\begin{aligned} \frac{NH_g[\omega_i]}{\rho_0 V} = & \frac{1}{V} \left\{ d\mathbf{r} \sum_i \phi_i(\mathbf{r}) \omega_i(\mathbf{r}) - \frac{1}{2} \sum_{i,j} \chi N_{ij} \phi_i(\mathbf{r}) \phi_j(\mathbf{r}) \right. \\ & + \eta \left[\sum_i \phi_i(\mathbf{r}) - 1 \right] - \frac{\gamma N}{2} \mathbf{T}(\mathbf{r}) : \mathbf{T}(\mathbf{r}) + \mathbf{M}(\mathbf{r}) : \mathbf{M}(\mathbf{r}) \left. \right\} \\ & - Q_x - e^{-F_B} N^{-1} Q_X \end{aligned} \quad (10)$$

where χN_{ij} represents the repulsive interaction between i and j ($i, j \in \{A, B, R\}$) and γN is the Maier-Saupe orientational interaction parameter. $\omega_i(\mathbf{r})$ and $\mathbf{M}(\mathbf{r})$ are the conjugated potential fields of total densities $\phi_i(\mathbf{r})$ and orientational order parameter $\mathbf{T}(\mathbf{r})$. Q_m is the single-chain partition function of m molecule, and the incompressibility of the system is ensured by $\eta(\mathbf{r})$. The standard SCFT derivation is implemented similar to our previous research.³² The SCFT equations are solved numerically.

In this study, the same component proportions of three blocks (coil-A, coil-B, and rod-R as shown in Figure 1) in X and x molecules ensure that macrophase segregation can hardly occur.^{18,19} In our system, the phase behavior is driven by parameters including β , the volume fraction of component i , f_i ($i = A, B, C$, i.e., coil-A, coil-B, and rod-R), and the orientation interaction parameter between rods γN . The parameter β describes the aspect ratio of rod ($\beta = \sqrt{6N} b/a$ is geometrical asymmetry between the rods and coils, where b is the length of one rod segment and a is the statistical segment length of the coil chains), and the rod chain with large β is long and thin, while the rod with small β is short and stumpy. All the lengths in our calculations are scaled by $R_g = \sqrt{N/6} a$, the unperturbed radius of gyration of coil chain. To obtain two-dimensional tiling patterns with microphase segregation and avoid other phases such as lamellae and hexagonal cylinder, the parameters in this study are specially selected. In detail, we set $\gamma N = 10$ to avoid lamellar phase and $N = 100$ to satisfy our

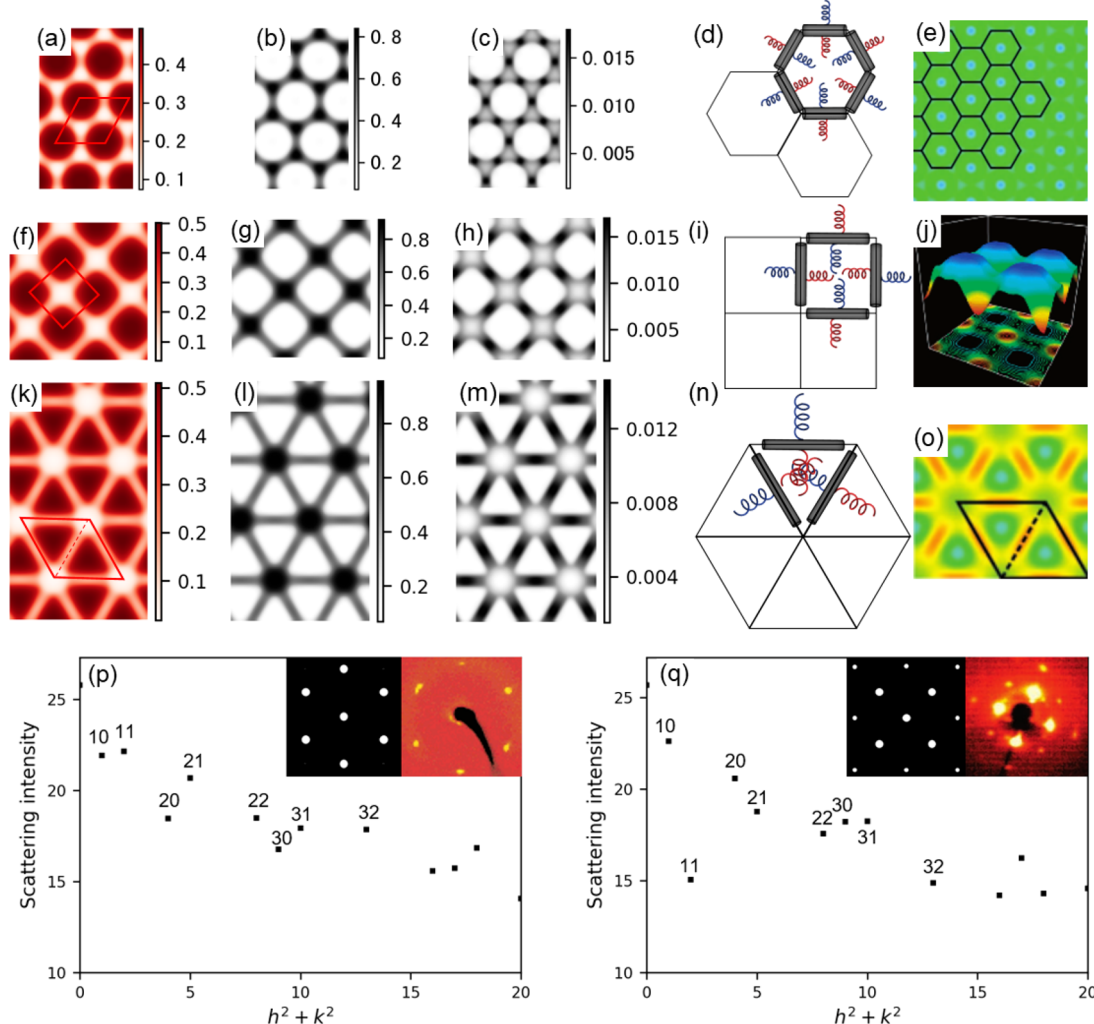


Figure 2. Three regular Archimedean tilings, $[6^3]$, $[4^4]$, and $[3^6]$ at $\beta = 12$, $f_R = 0.32$, $\beta = 14$, $f_R = 0.36$, and $\beta = 16$, $f_R = 0.40$, respectively. Other parameters are $\chi N_{AB} = 10$, $\chi N_{AR} = \chi N_{BR} = 70$, and $f_A = f_B = (1 - f_R)/2$. Density distributions of coil-A, rod, and junction points and schematic representations of molecular arrangements of (a–d) $[6^3]$, (f–i) $[4^4]$, and (k–n) $[3^6]$ tiling patterns. ED maps of (e) $[6^3]$ and (o) $[3^6]$ phases in the experiment of Zeng et al.²¹ and (j) $[4^4]$ phase in the experiment of Chen et al.¹⁸ Spectral analysis of (p) $[6^3]$ and (q) $[4^4]$; scattering intensities were simulated from the coil-A density distributions in (a and f) where the scattering peaks were labeled by the reciprocal vector lattice indexes h and k . The left insets in (p and q) are the corresponding two-dimensional scattering intensities. The right insets in (p and q) are the actual X-ray diffraction patterns of $[6^3]$ phase in the experiment of Kölbel et al.²⁰ and $[4^4]$ phase in the experiment of Chen et al.,¹⁹ respectively.

computational accuracy, and if not specially mentioned, $F_b = -5$ to ensure that X molecules dominate the system.

The simplest X-shaped molecule as shown in Figure 1 is used in our model. Notably in experiments, extra terminal chains were added to the end of rigid cores (the rod schematically shown in Figure 1, mostly aromatic chains) to increase the solubility or decrease the melting point of X/T-shaped rod-coil molecules, for example, terminal alkyl chains in facial amphiphiles^{19,33} or hydrogen-bonding groups, typically glycerol in bola-amphiphiles;^{21,34} the optional molecules are shown in Figure S2. The generalization of our method to other widely investigated molecules in experiments is straightforward. Besides, the simulation results of this study can be applied to those molecules, as discussed later.

RESULTS AND DISCUSSION

Regular Archimedean Tilings. Three simplest tilings composed of identical polygons and classified as regular tilings are obtained: $[6^3]$, $[4^4]$, and $[3^6]$ (Figure 2). In SCFT, the

density distribution of each component can be obtained, and thus we can speculate the molecular packing as well as rod arrangement. The density distributions of two mixed side chains are similar to each other; hence, only the density distribution of coil-A is shown. From Figure 2, the coil domains and surrounding rod frames show that the coil blocks form periodically arranged polygons and the rod blocks form mesh grids surrounding the coil domains. From the SCFT calculations, the edge lengths of polygons are 1.33, 2.19, and $3.10 R_g$, which are about equal to the rod lengths 1.92, 2.52, and $3.20 R_g$ in $[6^3]$, $[4^4]$, and $[3^6]$, respectively (the slight differences will be discussed later). In addition, the junction points of three blocks, i.e., the centers of rods, are rich at the midpoint of polygonal edges (Figures 2c, 2h, and 2m). According to the orientation distribution of rods (see the rod orientation of $[3^6]$ tiling in Figure S3), the main orientation is along the frames with some fluctuation. Therefore, the molecular arrangements in these tiling patterns can be suggested as schematically shown in Figures 2d, 2i, and 2n.

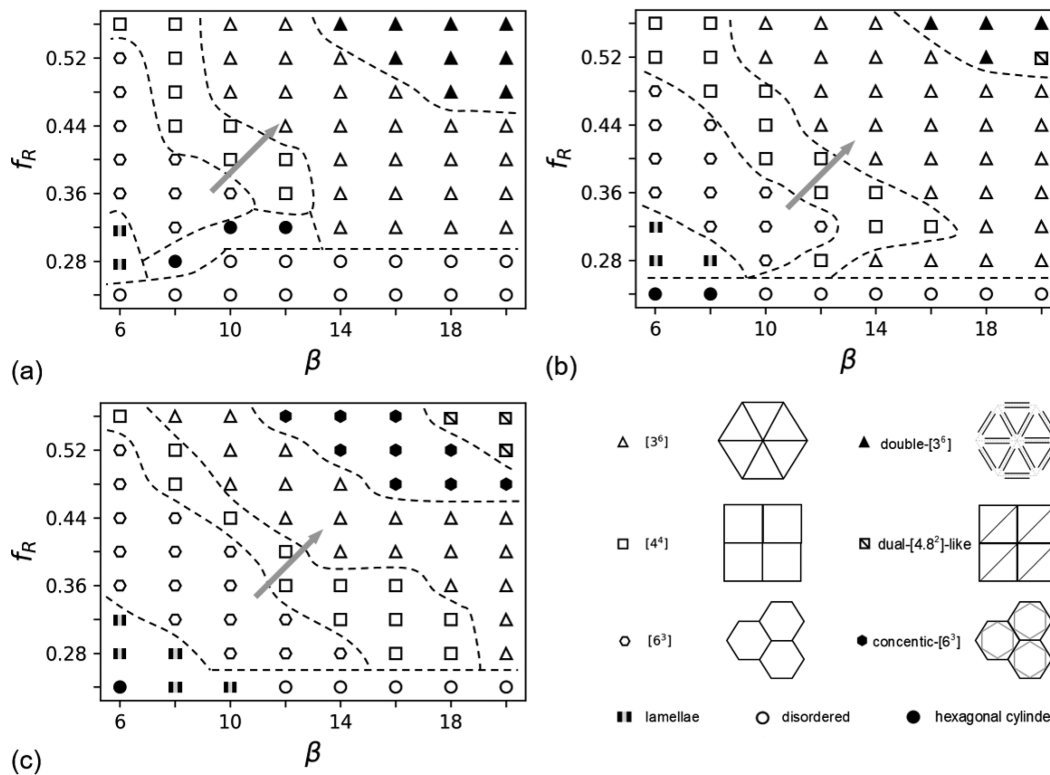


Figure 3. β - f_R phase diagrams at $\chi N_{\text{AR}} = \chi N_{\text{BR}} =$ (a) 60, (b) 70, and (c) 80. Other parameters are $\chi N_{\text{AB}} = 10$ and $f_A = f_B$. The hexagonal cylinder phase is shown in Figure S8. The dashed lines are a guide to the eye.

The self-assembly process that X-shaped macromolecules self-assemble into various tiling patterns can be considered as an engineering construction, where the rods make the polygonal frames and the side chains fill the inner spaces.^a It is noted that we compare the free energy of different structures and consider the one with the lowest energy as stable phase. Unless we say otherwise, the structures in the present work are stable states. Besides, we only focus on Archimedean tilings consisting of regular polygons; other novel non-Archimedean tilings, such as the ordinary [4.8]³⁶, octagon + pentagon, and pentagon + hexagon³⁷ patterns observed in experiment which consist of nonregular polygons, are also interesting works yet are beyond our scope in the present work. More complex Archimedean tiling patterns, such as [3³.4²] and [3⁴.6] tiling patterns, can be obtained by SCFT by design of more complex molecules, and the work is under way.

The obtained regular tiling patterns are consistent with experimental results. Zeng et al. obtained [6^3] and [3^6] tilings [ED (reconstructed electron) maps of hexagonal and triangular honeycombs in Figures 2e and 2o] using X-shaped bolaamphiphiles;²¹ they are identical to [6^3] and [3^6] tiling patterns shown in Figures 2a–d and 2k–n, respectively. The [4^4] tiling pattern shown in Figures 2f–i is also consistent with the ED map of T-shaped molecules in the experiment of Chen et al.³⁸ (Figure 2j). For a more quantitative insight into these tiling patterns, the Fourier transformations of density profiles for coil-A of [6^3] and [4^4] are identified, as shown in Figures 2p and 2q, in a similar manner discussed for other structures by Erukhimovich et al.³⁹ and Tang et al.⁴⁰ The plots are consistent with the actual X-ray diffraction patterns obtained experimentally^{21,38} as shown in the right insets in Figures 2p and 2q. The consistency between experiments and our calculations shows that the tiling patterns obtained by us are

indeed the honeycomb structures observed in the experiments.^{19,21}

Other than the one-color tiling pattern shown in Figure 2, where the two side chains are mixed together, two-color [3⁶] and [4⁴] tilings, where the two side chains are segregated into different domains (Figure S4), are also observed at a higher χN_{AB} ; namely, the repulsive interactions between coil-A and coil-B are very large. The phase segregation of two side chains manifests different symmetries (transform from *p6m* to *p3m1* for [3⁶] and *p4m* to *pgg* for [4⁴]) while the domain sizes remain the same. The alternatively arranged triangle or square domains may provide new characteristics to these functional materials. Because of the frustration (two side chains must mix together in a part of hexagons, see Figure S5) in [6³] tiling,²¹ a much larger χN_{AB} is needed to form two- or three-color [6³] tiling patterns with segregated side chains. However, a larger value of χN demands much more computer cost which is beyond our current computational capabilities. Surprisingly, in the phase diagrams shown in Figure 3, we observe a special [6³] tiling as shown in Figures 4a–e for the first time and name as concentric-[6³] tiling, where the rods form two concentric hexagons with 30° rotation angle and the inner small hexagon's vertexes are located at the centers of outer hexagon's edges, as shown in Figure 4e and the inset of Figure 4b. Similar to the hexagonal columns phase, i.e., Figure 10c in the work by Chen et al.,¹⁸ the rod chains in the concentric-[6³] tiling are arranged around the coil domains, yet unlike the rod chains with random orientations in the hexagonal columns in their work, the rod chains keep the end-to-end correlations and form two neighboring frames of the hexagon.

Non-Regular and Dual Archimedean Tilings. It is interesting and challenging to find all 11 kinds of Archimedean tilings. Some tilings are inaccessible by the directed self-

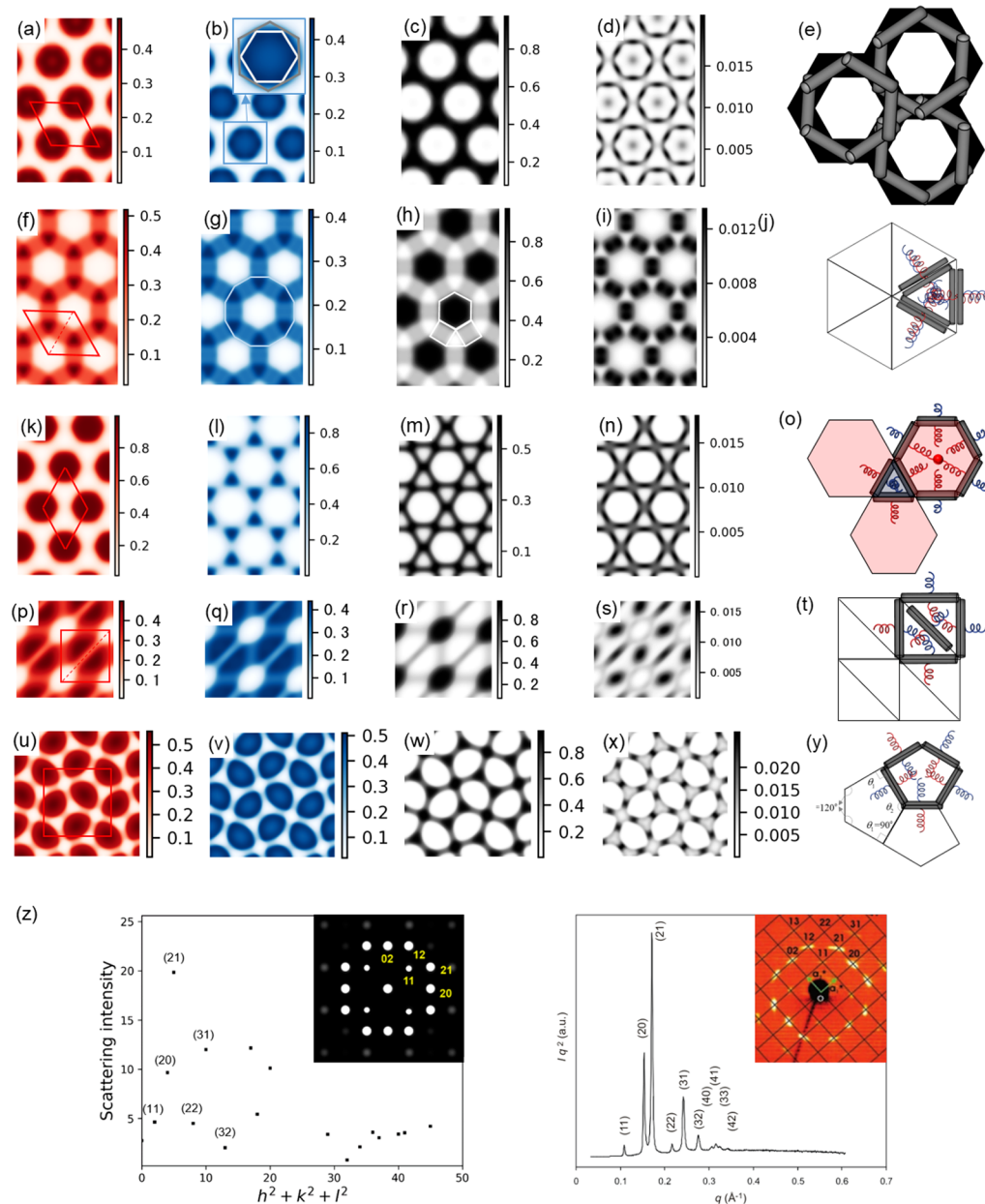


Figure 4. Density distributions of coil-A, coil-B, rod, and junction points and the schematic representations of molecular arrangements of (a–e) concentric- $[6^3]$ tiling at $\beta = 18$, $f_R = 0.52$, $f_A = f_B = 0.24$, $\chi N_{AB} = 10$, $\chi N_{AR} = \chi N_{BR} = 80$; (f–j) double- $[3^6]$ tiling at $\beta = 14$, $f_R = 0.56$, $f_A = f_B = 0.22$, $\chi N_{AB} = 10$, $\chi N_{AR} = \chi N_{BR} = 60$; (k–o) $[(3.6)^2]$ tiling at $\beta = 12$, $f_R = 0.28$, $f_A = 0.48$, $f_B = 0.24$, $\chi N_{AB} = \chi N_{AR} = \chi N_{BR} = 60$; (p–t) dual- $[4.8^2]$ -like tiling at $\beta = 20$, $f_R = 0.40$, $f_A = f_B = 0.30$, $\chi N_{AB} = 10$, $\chi N_{AR} = \chi N_{BR} = 70$; and (u–y) dual- $[3^2.4.3.4]$ tiling at $\beta = 14$, $f_R = 0.32$, $f_A = f_B = 0.34$, $\chi N_{AB} = 10$, $\chi N_{AR} = \chi N_{BR} = 90$, respectively. (z) Left panel shows the scattering intensity simulated from the coil-A density distribution in (u), and the right panel shows the actual X-ray diffraction pattern of dual- $[3^2.4.3.4]$ tiling in the experiment of Chen et al.¹⁹ The insets show the corresponding two-dimensional scattering intensities.

assembly of certain molecules or unnecessary to do so due to the synthetic challenge. Then, indirect approaches are needed, including but not limited to recombination tilings,^{13,19} which detach and recombine polygons into new ones (Figure S6), and dual-tilings, which consider the centers of each polygon in tilings as vertexes and join the centers of adjacent polygons,⁴¹ i.e., replace the tiling centers by vertices²¹ (Figure S7).

The double- $[3^6]$ tiling pattern, where one polygonal edge consists of two completely interdigitated rods with side by side packing (Figure 4j), is observed at a large β as shown in Figures 3a,b. Experimentally, tiling patterns with one polygonal edge constructed by two side by side packing rods can be

obtained by T-shaped molecules,⁴² yet the double- $[3^6]$ tiling is first found by X-shaped molecules in our investigation. The novel structure contains three different domains: triangle domains (mixed coil-A and coil-B), square domains (mixed coil-A, coil-B, and rod), and hexagon domains (rod) as shown in Figures 4f–h. If these three domains are taken as independent polygons, the double- $[3^6]$ turns into the $[3.4.6.4]$ tiling pattern. It is noted that the hexagon and surrounding six triangles and six squares form a large regular 12-gon (Figure 4g). The combination of several small polygons into a large polygon (see Figure S6) is a promising way to

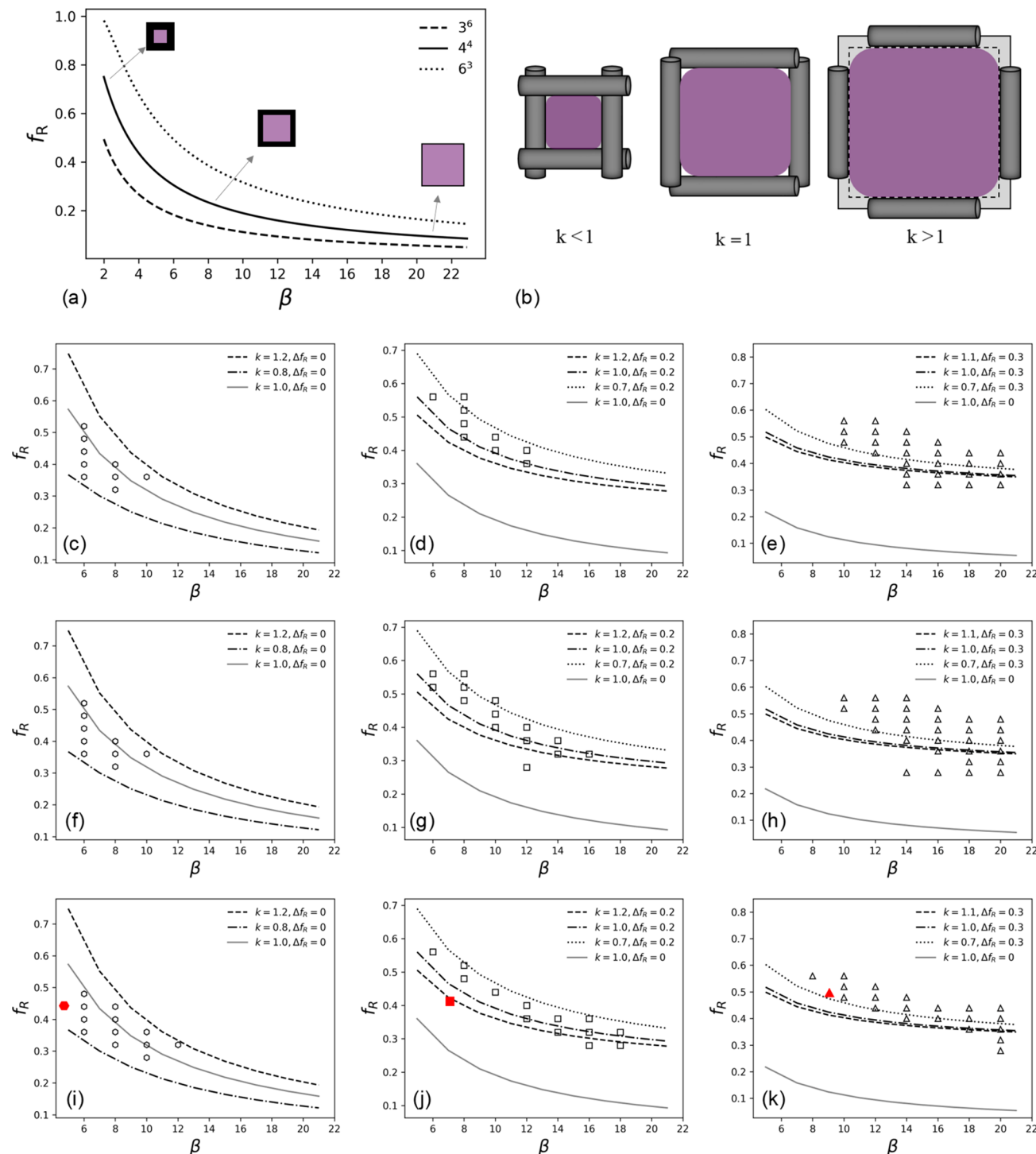


Figure 5. (a) Relationship between the length-to-diameter ratios β and volume fraction f_R of end-to-end linked rod blocks in $[6^3]$, $[4^4]$, and $[3^6]$ tiling patterns. The insets show the schematic representations of arrangement of rods with different β values for $[4^4]$ tiling. (b) Schematic illustration of rod arrangements in the $[4^4]$ tiling pattern with the purple and gray regions representing coil and rod phases, respectively. We compared the SCFT results, $\beta-f_R$ fit lines, and experimental results in (c–k); the black hollowed hexagons, squares, and triangles are $[6^3]$, $[4^4]$, and $[3^6]$ tiling patterns in (c–e) Figure 3a, $\chi N_{\text{AR}} = \chi N_{\text{BR}} = 60$, (f–h) Figure 3b, $\chi N_{\text{AR}} = \chi N_{\text{BR}} = 70$, and (i–k) Figure 3c, $\chi N_{\text{AR}} = \chi N_{\text{BR}} = 80$, respectively. The red solid hexagon, square, and triangle in (i–k) are the estimated parameters of molecules in experiments.^{19,21}

obtain tilings containing n -polygons ($n > 6$) such as $[4.6.12]$, $[4.8^2]$, and $[3.12^2]$.

Dual- $[4.8^2]$ -like (right upper corners in Figures 3b,c) and dual- $[3^2.4.3.4]$ are found at relatively large χN between the rod and coil species, such as $\chi N_{\text{AR}} = \chi N_{\text{BR}} = 90$. The dual- $[4.8^2]$ -like tiling pattern shown in Figures 4p–t contains two types of

rods, i.e., the rods located at edges and rods located at diagonal lines, which seems to add an extra rod packing at the diagonal line of each square in the $[4^4]$ tiling pattern. A comparison between the lengths of rods ($4R_g$) and square edges ($2.7R_g$) shows that the rods located at the edges partially overlap with each other while the rods located at the diagonal lines barely

not. Moreover, unlike dual-[4.8²] (Figure S7) where the diagonals have two perpendicular directions, the dual-[4.8²]-like tiling pattern found in our investigation contains diagonal rods with identical directions. This is found for the first time. Besides, a metastable phase dual-[3².4.3.4] (stable state is [4⁴]) is also observed as shown in Figures 4u–y. The scattering intensity simulated from the density profile of coil-A is identical to the actual X-ray diffraction patterns of the *p4gm* phase in the experiment of Chen et al.¹⁹ as shown in Figure 4z.

Apart from three regular tilings shown in Figure 2, other eight Archimedean tilings contain more than one type of polygons (see Figure S1); it is straightforward to associate the X-shaped molecules with unbalanced side chains. The [(3.6)²] tiling pattern is observed as shown in Figures 4k–o, consistent with experiments⁴³ and simulations.^{43,44} Coil-A and coil-B blocks are separated into hexagon and triangle domains in a 1:2 ratio.^c The formation of [(3.6)²] proves the validity of unbalanced side chains in the formation of other tiling patterns including [3.12²], [3.4.6.4], [4.6.12], [4.8², [3².4.3.4], [3³.4²], and [3⁴.6], as shown in Figure S1. We note that unlike standard Archimedean tilings, the rod chains as edges in the tiling patterns formed by X-shaped rod-coil macromolecules can slightly distort, commonly observed in experiments.⁴⁵ For example, the [(3.6)²] pattern in Figures 4k–o is not composed of standard geometrical edge-to-edge hexagons and triangles. In addition, a distorted [4⁴] tiling is also shown in Figure S9. The distorted tilings are also classified as Archimedean tiling patterns in this study, and they will be discussed latter.

Formation Mechanism for Tiling Patterns. Experimentally, it was inferred that changing the length of lateral chains influenced the diameter of columns, thus determining the number of rod chains required to surround these columns.^{18,45,46} Zeng et al. proposed that the formation of tiling patterns depends on the ratio of cubic root of coil chain volume and the length of rod chain.²¹ Our study also demonstrates that with the increase in the length of rods $L_r = \beta f_R/2$ in units of R_g as shown in the gray arrows in Figure 3, the phase transforms from [6³] to [4⁴] and finally to [3⁶], consistent with the experimental studies.^{18,21,45,46} Yet, experimental investigations on the effect of radial dimensions by changing the lateral dimension of rigid cores are inconvenient due to synthetic difficulties, and thus the lateral dimensions of rods are generally constant in these investigations.⁴² The estimated β of rods, i.e., length-to-diameter ratios of rigid cores in experiments, are generally 4–10,^{19,21} which indicates that the length is not large enough to ignore the diameter of rods. One should consider not only the length of rigid cores and polygonal area of different tiling patterns (see Figure S10) but also the length-to-diameter ratio of the rod chains in the investigation of the fabrication of tiling patterns. Considering the harsh self-assembly conditions, systematic experimental investigation is an impossible task. A clearer quantitative/semitquantitative guiding principle than previous empirical rules^{18,21–23,25,45,46} for the explanation and prediction of the fabrication of different tiling patterns is needed. In this study, by calculating the phase diagrams (Figure 3) of X-shaped rod-coil molecules, we propose a semiquantitative $\beta-f_R$ mechanism to explain and predict the formation of Archimedean tiling patterns.

In SCFT calculation, s_i the proportion of domain size of component i in the density distribution map should equal to f_i , i.e., the volume fraction of i ($i = A, B, R$). Taking the [4⁴] tiling pattern where the rods arrange end-to-end as an example, $s_A +$

$s_B = (S_A + S_B)/S_{\text{total}} = f_A + f_B = 1 - f_R$. $S_{\text{total}} = L_r^2$ is the area of square ($L_r = \beta f_r$ is the length of a single rod, i.e., the edge length of squares, where $f_r = f_R/2$ is the volume fraction of a single rod), and $S_A + S_B$ is the area of red inner square surrounded by black edges as shown in the insets of Figure 5a. β is assumed to be the length-to-diameter ratio of rod chains in the present work; thus, a simple mechanism regarding the $\beta-f_R$ relation is proposed: if the [4⁴] tiling pattern is formed, β and f_R should satisfy $f_R = \frac{2}{\beta} - \frac{1}{\beta^2}$ (see detailed derivation in Figure S11). Similarly, $f_R = \frac{2\sqrt{3}}{\beta} - \frac{3}{\beta^2}$ for [6³] and $f_R = \frac{2\sqrt{3}}{3\beta} - \frac{1}{3\beta^2}$ for [3⁶] as shown in Figure 5a. Considering the flexibility and complexity of self-assembly of rod-coil molecules, the $\beta-f_R$ relation should be modified.

First, during the formation of diverse tiling patterns by X-shaped rod-coil polymers, the entropy of lateral chains dominates the system. To satisfy the space requirement of lateral chains, rod blocks may overlap with each other or separate from each other. A new parameter $k = L_{\text{edge}}/L_r$ is proposed to describe the arrangement of adjacent rod blocks in the same line. Three situations, $k < 1$, $k = 1$, and $k > 1$, representing overlapped rods, end-to-end rods, and separated rods in tiling patterns, respectively, are shown in Figure 5b. Second, although SCFT has achieved tremendous success in predicting the phase behavior of various copolymers, deviations may be produced when using SCFT to X-shaped rod-coil copolymers with short chains. On one hand, the results of SCFT, a field theory method, are density distributions, where the polygons have rounded corners due to incompressible melt constraint (see Figures 2b, 2g, and 2i) rather than the sharp corners found in experiments (Figure 5b, $k > 1$). We can denote the mismatch between the corner shape in SCFT and experiments as the corner effect. This is supposed to decrease with increasing χN as larger interactions between coil chains and rods result in sharper interfaces. As the density of rounded corners in regular n -side polygons is $4 \tan(\pi/n)/L_{\text{edge}}^2$, the corner effect decreases with the increase in the number of edges. On the other hand, the shape of rod chains, overlap of rods, and local cavity in the molecular packing as shown in the CPK (space-filling) model in the study of Cheng et al.⁴⁵ may also cause the mismatch between f_R in our calculation and the actual volume fraction of rod chains in experiments. Therefore, another parameter Δf_R is proposed to offset the deviation. Considering k as shown in Table S1 and the different corner effects, Δf_R is set as 0, 0.2, and 0.3 for [6³], [4⁴], and [3⁶] in Figures 5c–k, respectively.

A comparison among $\beta-f_R$ fit lines, three regular tiling patterns in Figure 3, and experimental results shown in Figure 5 shows that the SCFT and experimental results are consistent with the $\beta-f_R$ lines revised by k and Δf_R . The [6³] and [4⁴] shown in Figures 5c, 5f, and 5i and Figures 5d, 5g, and 5j are in the range of revised $\beta-f_R$ lines. With the increase in χN , the [3⁶] tiling patterns are more in line with the revised $\beta-f_R$ lines, as shown in Figures 5e, 5h, and 5k. Thus, a one-step solution is proposed: the formation of various tiling patterns is controlled by the $\beta-f_R$ lines that can be revised by two parameters, k and Δf_R . The value of Δf_R is determined by the edges of polygons in tiling patterns, and the value of k is determined by the overlap of rod chains, depending on particular molecules. For example, bola-amphiphiles with hydrogen-bonding groups at the terminals of rods provide extra interactions between rod

blocks; this may influence $\beta-f_R$ lines. Facial amphiphiles with extra alkyl chains at the terminals of rods will increase k , as the terminal chains that separate the adjacent rods are generally located at the vertexes of polygons (the corners shown in Figure 5b, $k > 1$). The estimated β and f_R values of the molecules in [6³] and [3⁶] tiling patterns self-assembled by X-shaped bola-amphiphiles in the experiment of Zeng et al.²¹ and the [4⁴] tiling pattern by T-shaped facial amphiphiles in the experiment of Chen et al.¹⁹ (solid red polygons in Figures 5i–k) are perfectly consistent with the results of this study. The perfect matching between $\beta-f_R$ lines and experiments indicates that the mechanism can be extended to other molecules, such as X/T-shaped facial amphiphiles and bola-amphiphiles. This study also demonstrates that the effective components in X-shaped molecules are only the rigid cores and side chains, and other components, which facilitate the melt or dissolution of these molecules, only play a supplementary role.

Influence of Hydrogen Bonds on the Scale of Microphase Separation. For many applications of polymers such as microelectronic and optoelectronic devices, a smaller domain size usually means a better performance and efficiency. Thus, the microstructure with a smaller size is the key to enhance and expand the application of polymers. For X-shaped rod-coil molecules, the domain size mainly depends on the shape of polygons and volume of flexible side chains. Obviously, the area difference between different polygons in Archimedean tiling patterns leads to different domain sizes. Yet this part is fixed, and no further optimization can be done. The overlap of rod blocks can also determine the scale of microphase separation discussed previously. To reduce the scale of microphase structures in Archimedean tiling patterns formed by X-shaped molecules, the length of side chains should be reduced and the microphase separation structures should be maintained at the same time. Hydrogen bonds widely used to control the phase behavior of polymers for a long time may help to achieve our propose.⁴⁷ The effect of hydrogen bonds on the self-assembly behavior is calculated as shown in Figure 6. With increasing of hydrogen bond energy $F_b(z_X)$, the system turns from disordered phases to [4⁴] tiling patterns, indicating that hydrogen-bond formation can facilitate the microphase separation behavior. This is because hydrogen bonds provide extra attractions in coil-A domains, thus increasing the effective interaction parameter χN_{eff}

between coil-A and other components. Moreover, the decrease in N (number of segments of molecule X) increases the concentration of hydrogen-bonding groups, thus increasing the ratio of molecules X and further reducing the domain size. We note that in experiments N can be much smaller than 100, requiring quite large χ to occur microphase separation, which is beyond our current computational capabilities. Thus, the reduction in domain size resulting from hydrogen-bond formation can be more significant experimentally.

CONCLUSIONS

In this study, SCFT is implemented into X-shaped rod-coil supra-macromolecules. Five (dual) tiling patterns including [6³], [4⁴], [3⁶], [(3.6)²], and dual-[3².4.3.4] are obtained, highly consistent with experiments. In particular, novel tiling patterns including concentric-[6³], [3.4.6.4], and dual-[4.8²]-like self-assembled by X-shaped molecules are discovered for the first time. Furthermore, a simple and valid $\beta-f_R$ mechanism is proposed to explain and predict the formation of Archimedean tiling patterns. In detail, the formation of tiling patterns depends on the relationship between two essential parameters, the long diameter ratio β , and volume fractions of rod blocks f_R . The mechanism can be generalized to other molecules such as X/T-shaped bola-amphiphiles and facial amphiphiles widely investigated experimentally. This study is a starting point for establishing a platform for macromolecular tiling via X-shaped rod-coil supra-macromolecules.

ASSOCIATED CONTENT

Supporting Information

The Supporting Information is available free of charge on the ACS Publications website at DOI: [10.1021/acs.macromol.8b01078](https://doi.org/10.1021/acs.macromol.8b01078).

Figures S1–S11, Table S1 (PDF)

AUTHOR INFORMATION

Corresponding Author

*E-mail: pingtang@fudan.edu.cn (P.T.).

ORCID

Ping Tang: 0000-0003-0253-1836

Notes

The authors declare no competing financial interest.

ACKNOWLEDGMENTS

The authors thank the National Natural Science Foundation of China for financial support (Grants 21574027, 21774027, and 21534002).

ADDITIONAL NOTES

^aThe tiling patterns are similar to steel-reinforced cement; therefore, the mechanical properties of these polymer tiling patterns are notable. In fact, Souslov et al.³⁵ proved the distinct mechanical properties of different tiling patterns resulting from diverse polygons and different symmetries.

^bConsidering the structure correlation between tiling and dual tiling patterns as shown in Figures S1 and S7, if the functional sites are changed from the coil side chains to the terminal of rod chains in X-shaped molecules, dual tiling patterns can replace the corresponding tiling patterns in practical applications.

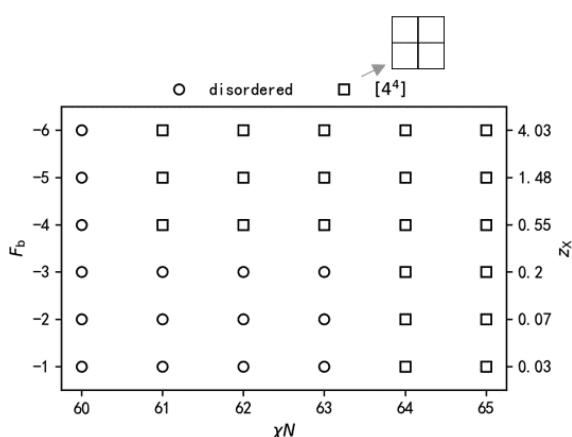


Figure 6. $\chi N - F_b(z_X)$ phase diagram at $\chi N_{AB} = 10$, $\chi N_{AR} = \chi N_{BR} = \chi N$, $\beta = 12$, $f_R = 0.32$, and $f_A = f_B = 0.34$.

$[(3.6)^2]$, also named the Kagome lattice, represents a basket with holes in Japanese. Besides the aesthetic value, the novel structure can be applied into spin-frustrated magnetic materials.⁴³ Moreover, the $[(3.6)^2]$ tiling shows peculiar mechanical properties in the study of Souslov et al.³⁵

■ REFERENCES

- (1) Kepler, J. *Harmonices Mundi*; Linz: 1619.
- (2) Lee, S.; Bluemle, M. J.; Bates, F. S. Discovery of a Frank-Kasper σ phase in sphere-forming block copolymer melts. *Science* **2010**, *330*, 349–353.
- (3) Urgel, J. I.; Écija, D.; Lyu, G.; Zhang, R.; Palma, C.-A.; Auwärter, W.; Lin, N.; Barth, J. V. Quasicrystallinity expressed in two-dimensional coordination networks. *Nat. Chem.* **2016**, *8*, 657.
- (4) Sirringhaus, H.; Tessler, N.; Friend, R. H. Integrated optoelectronic devices based on conjugated polymers. *Science* **1998**, *280*, 1741–1744.
- (5) Wang, D.; Caruso, F. Fabrication of polyaniline inverse opals via templating ordered colloidal assemblies. *Adv. Mater.* **2001**, *13*, 350–354.
- (6) Hagleitner, C.; Hierlemann, A.; Lange, D.; Kummer, A.; Kerness, N.; Brand, O.; Baltes, H. Smart single-chip gas sensor microsystem. *Nature* **2001**, *414*, 293–296.
- (7) Choi, D.-G.; Jang, S. G.; Yu, H. K.; Yang, S.-M. Two-Dimensional Polymer Nanopattern by Using Particle-Assisted Soft Lithography. *Chem. Mater.* **2004**, *16*, 3410–3413.
- (8) Sochnikov, I.; Shaulov, A.; Yeshurun, Y.; Logvenov, G.; Bozovic, I. Large oscillations of the magnetoresistance in nanopatterned high-temperature superconducting films. *Nat. Nanotechnol.* **2010**, *5*, 516–519.
- (9) Ryu, D. Y.; Shin, K.; Drockenmuller, E.; Hawker, C. J.; Russell, T. P. A generalized approach to the modification of solid surfaces. *Science* **2005**, *308*, 236–239.
- (10) Krumeich, F.; Conrad, M.; Nissen, H.-U.; Harbrecht, B. The mesoscopic structure of disordered dodecagonal tantalum telluride: a high-resolution transmission electron microscopy study. *Philos. Mag. Lett.* **1998**, *78*, 357–367.
- (11) Atwood, J. L. Kagome lattice: a molecular toolkit for magnetism. *Nat. Mater.* **2002**, *1*, 91–92.
- (12) Zhang, F.; Liu, Y.; Yan, H. Complex Archimedean tiling self-assembled from DNA nanostructures. *J. Am. Chem. Soc.* **2013**, *135*, 7458–7461.
- (13) Miyase, H.; Asai, Y.; Takano, A.; Matsushita, Y. Kaleidoscopic tiling patterns with large unit cells from ABC star-shaped terpolymer/diblock copolymer blends with hydrogen bonding interaction. *Macromolecules* **2017**, *50*, 979–986.
- (14) Tang, P.; Qiu, F.; Zhang, H.; Yang, Y. Morphology and phase diagram of complex block copolymers: ABC linear triblock copolymers. *Phys. Rev. E* **2004**, *69*, 031803-1–031803-8.
- (15) Tang, P.; Qiu, F.; Zhang, H.; Yang, Y. Morphology and phase diagram of complex block copolymers: ABC star triblock copolymers. *J. Phys. Chem. B* **2004**, *108*, 8434–8438.
- (16) Cushen, J. D.; Bates, C. M.; Rausch, E. L.; Dean, L. M.; Zhou, S. X.; Willson, C. G.; Ellison, C. J. Thin film self-assembly of poly(trimethylsilylstyrene-*b*-_{D,L}-lactide) with sub-10 nm domains. *Macromolecules* **2012**, *45*, 8722–8728.
- (17) Poelma, J. E.; Ono, K.; Miyajima, D.; Aida, T.; Satoh, K.; Hawker, C. J. Cyclic block copolymers for controlling feature sizes in block copolymer lithography. *ACS Nano* **2012**, *6*, 10845–10854.
- (18) Chen, B.; Baumeister, U.; Pelzl, G.; Das, M. K.; Zeng, X.; Ungar, G.; Tschierske, C. Carbohydrate rod conjugates: ternary rod-coil molecules forming complex liquid crystal structures. *J. Am. Chem. Soc.* **2005**, *127*, 16578–16591.
- (19) Chen, B.; Zeng, X.; Baumeister, U.; Ungar, G.; Tschierske, C. Liquid crystalline networks composed of pentagonal, square, and triangular cylinders. *Science* **2005**, *307*, 96–99.
- (20) Kölbel, M.; Beyersdorff, T.; Cheng, X. H.; Tschierske, C.; Kain, J.; Diele, S. Design of liquid crystalline block molecules with nonconventional mesophase morphologies: calamitic bolaamphiphiles with lateral alkyl chains. *J. Am. Chem. Soc.* **2001**, *123*, 6809–6818.
- (21) Zeng, X.; Kieffer, R.; Glettner, B.; Nürnberger, C.; Liu, F.; Pelz, K.; Prehm, M.; Baumeister, U.; Hahn, H.; Lang, H.; Gehring, G. A.; Weber, C. H. M.; Hobbs, J. K.; Tschierske, C.; Ungar, G. Complex multicolor tilings and critical phenomena in tetraphilic liquid crystals. *Science* **2011**, *331*, 1302.
- (22) Crane, A. J.; Martínez-Veracoechea, F. J.; Escobedo, F. A.; Müller, E. A. Molecular dynamics simulation of the mesophase behaviour of a model bolaamphiphilic liquid crystal with a lateral flexible chain. *Soft Matter* **2008**, *4*, 1820–1829.
- (23) Bates, M.; Walker, M. Dissipative particle dynamics simulation of T- and X-shaped polyphilic molecules exhibiting honeycomb columnar phases. *Soft Matter* **2009**, *5*, 346–353.
- (24) Nguyen, T. D.; Glotzer, S. C. Reconfigurable assemblies of shape-changing nanorods. *ACS Nano* **2010**, *4*, 2585–2594.
- (25) Liu, X.; Yang, K.; Guo, H. Dissipative Particle dynamics simulation of the phase behavior of T-Shaped ternary amphiphiles possessing rodlike mesogens. *J. Phys. Chem. B* **2013**, *117*, 9106–9120.
- (26) Tschierske, C.; Nurnberger, C.; Ebert, H.; Glettner, B.; Prehm, M.; Liu, F.; Zeng, X.-B.; Ungar, G. Complex tiling patterns in liquid crystals. *Interface Focus* **2012**, *2*, 669–680.
- (27) Tschierske, C. Development of structural complexity by liquid-crystal self-assembly. *Angew. Chem., Int. Ed.* **2013**, *52*, 8828–8878.
- (28) Yu, J.; Liu, F.; Tang, P.; Qiu, F.; Zhang, H.; Yang, Y. Effect of geometrical asymmetry on the phase behavior of rod-Coil diblock copolymers. *Polymers* **2016**, *8*, 184.
- (29) Feng, E. H.; Lee, W. B.; Fredrickson, G. H. Supramolecular diblock copolymers: a field-theoretic model and mean-field solution. *Macromolecules* **2007**, *40*, 693–702.
- (30) Fredrickson, G. *The Equilibrium Theory of Inhomogeneous Polymers*; Oxford University Press: 2006.
- (31) Dehghan, A.; Shi, A.-C. Modeling hydrogen bonding in diblock copolymer/homopolymer blends. *Macromolecules* **2013**, *46*, 5796–5805.
- (32) Liu, F.; Sun, T.; Tang, P.; Zhang, H.; Qiu, F. Understanding chain folding morphology of semicrystalline polymers based on a rod-coil multiblock model. *Soft Matter* **2017**, *13*, 8250–8263.
- (33) Kolbel, M.; Beyersdorff, T.; Sletvold, I.; Tschierske, C.; Kain, J.; Diele, S. Design of new mesogenic block molecules: formation of columnar mesophases by calamitic bolaamphiphiles with lateral lipophilic substituents. *Angew. Chem., Int. Ed.* **1999**, *38*, 1077–1080.
- (34) Tschierske, C. Liquid crystal engineering-new complex mesophase structures and their relations to polymer morphologies, nanoscale patterning and crystal engineering. *Chem. Soc. Rev.* **2007**, *36*, 1930–1970.
- (35) Souslov, A.; Liu, A. J.; Lubensky, T. C. Elasticity and response in nearly isostatic periodic lattices. *Phys. Rev. Lett.* **2009**, *103*, 205503.
- (36) Liu, F.; Kieffer, R.; Zeng, X.; Pelz, K.; Prehm, M.; Ungar, G.; Tschierske, C. Arrays of giant octagonal and square cylinders by liquid crystalline self-assembly of X-shaped polyphilic molecules. *Nat. Commun.* **2012**, *3*, 1114.
- (37) Poppe, S.; Lehmann, A.; Scholte, A.; Prehm, M.; Zeng, X.; Ungar, G.; Tschierske, C. Zeolite-like liquid crystals. *Nat. Commun.* **2015**, *6*, 8637.
- (38) Chen, B.; Baumeister, U.; Diele, S.; Das, M. K.; Zeng, X.; Ungar, G.; Tschierske, C. A new type of square columnar liquid crystalline phases formed by facial amphiphilic triblock molecules. *J. Am. Chem. Soc.* **2004**, *126*, 8608–8609.
- (39) Erukhimovich, I.; Kriksin, Y.; ten Brinke, G. Diamond-forming block copolymers and diamond-like morphologies: a new route toward efficient block copolymer membranes. *Macromolecules* **2015**, *48*, 7909–7922.
- (40) Tang, J.; Jiang, Y.; Zhang, X.; Yan, D.; Chen, J. Z. Y. Phase diagram of rod-coil diblock copolymer melts. *Macromolecules* **2015**, *48*, 9060–9070.
- (41) Robert, W. *The Geometrical Foundation of Natural Structure*; Dover: New York, 1979.

- (42) Kieffer, R.; Prehm, M.; Glettner, B.; Pelz, K.; Baumeister, U.; Liu, F.; Zeng, X.; Ungar, G.; Tschierske, C. X-shaped polyphilics: liquid crystal honeycombs with single-molecule walls. *Chem. Commun.* **2008**, 3861–3863.
- (43) Glettner, B.; Liu, F.; Zeng, X.; Prehm, M.; Baumeister, U.; Walker, M.; Bates, M. A.; Boesecke, P.; Ungar, G.; Tschierske, C. Liquid-crystalline kagome. *Angew. Chem., Int. Ed.* **2008**, *47*, 9063–9066.
- (44) Bates, M. A.; Walker, M. Dissipative particle dynamics simulation of quaternary bolaamphiphiles: multi-colour tiling in hexagonal columnar phases. *Phys. Chem. Chem. Phys.* **2009**, *11*, 1893–1900.
- (45) Cheng, X.; Prehm, M.; Das, M. K.; Kain, J.; Baumeister, U.; Diele, S.; Leine, D.; Blume, A.; Tschierske, C. Calamitic bolaamphiphiles with (semi)perfluorinated lateral chains: polyphilic block molecules with new liquid crystalline phase structures. *J. Am. Chem. Soc.* **2003**, *125*, 10977–10996.
- (46) Cheng, X.; Das, M. K.; Baumeister, U.; Diele, S.; Tschierske, C. Liquid crystalline bolaamphiphiles with semiperfluorinated lateral chains: competition between layerlike and honeycomb-like organization. *J. Am. Chem. Soc.* **2004**, *126*, 12930–12940.
- (47) Sijbesma, R. P.; Beijer, F. H.; Brunsved, L.; Folmer, B. J.; Hirschberg, J. K.; Lange, R. F.; Lowe, J. K.; Meijer, E. Reversible polymers formed from self-complementary monomers using quadruple hydrogen bonding. *Science* **1997**, *278*, 1601–1604.